Journal of Power Sources 210 (2012) 297–302

Contents lists available at SciVerse ScienceDirect

Journal of Power Sources

journal homepage: www.elsevier.com/locate/jpowsour

Defective mesoporous $Li_4Ti_5O_{12-y}$: An advanced anode material with anomalous capacity and cycling stability at a high rate of 20 C

Xiaomei Chen [a], Xiangfeng Guan [b], Liping Li [a], Guangshe Li [a,*]

[a] State Key Lab of Structural Chemistry, Fujian Institute of Research on the Structure of Matter, Chinese Academy of Sciences, Fuzhou 350002, People's Republic of China
[b] Key Lab of Coal to Ethylene Glycol and Its Related Technology, Fujian Institute of Research on the Structure of Matter, Chinese Academy of Sciences, Fuzhou 350002, People's Republic of China

ARTICLE INFO

Article history:
Received 19 December 2011
Received in revised form 5 March 2012
Accepted 7 March 2012
Available online 3 April 2012

Keywords:
Lithium-ion batteries
Lithium titanate
Defective
Mesoporous

ABSTRACT

How to obtain an excellent capacity and cycling stability of electrodes that work at high rates is now challenging the development of lithium-ion batteries. Herein, we initiate a facile solvothermal method to prepare defective mesoporous $Li_4Ti_5O_{12-y}$ as an anode material with an improved high-rate performance for lithium-ion batteries. The high-rate performance for the resultant anode is represented by a discharge capacity of 139 mAh g^{-1} at a high rate of 20 C with a capacity retention of 91.4% over 300 cycles. Different from the strategies popularly used in literature, the current approach does not rely on any aids from conductive layers or foreign dopants, but takes advantages of the unique features of a defective mesoporous structure with oxygen vacancies and Ti^{3+}–O^{2-}–Ti^{4+} pairs. These features enable an improved intrinsic electronic conductivity, which leads to a high-rate performance and cycling stability superior to the stoichiometric mesoporous counterpart when annealing in air. The defective mesoporous $Li_4Ti_5O_{12-y}$ is therefore demonstrated to be a promising advanced anode material for high-rate lithium-ion batteries.

1. Introduction

Lithium-ion batteries have drawn considerable attention for their broad class of important applications due to the high energy density, low cost, and high-rate capability [1,2]. For some practical applications like hybrid electric vehicles or electric vehicles, lithium ion batteries have to be re-charged very fast, and therefore the relevant electrode materials have to work at high rates, while maintaining the excellent capacity and cycling stability. Among all electrode materials, spinel $Li_4Ti_5O_{12}$ is a promising anode material for its good cycling stability, which is due to zero-strain properties during lithium ion insertion and extraction processes, and its relatively high potential at 1.55 V, which can effectively suppress the formation of solid-electrolyte interfaces, and thus providing an improved safety for lithium-ion batteries [3–5]. However, it is still very difficult to retain a high capacity and cycling stability at high rates, because electronic conductivity for $Li_4Ti_5O_{12}$ is usually very low, $<10^{-13}$ S cm^{-1} [6]. To improve the rate capability of $Li_4Ti_5O_{12}$, many efforts have been done, which include (i) preparation of small-sized $Li_4Ti_5O_{12}$ with various morphologies [7,8]; (ii) coating carbon or other conductive agents on the surface of $Li_4Ti_5O_{12}$ [3]; and (iii) doping foreign metal ions (e.g., V^{5+} [9], Sr^{2+} [10], Al^{3+} [11]) into the lattice of $Li_4Ti_5O_{12}$. All these suffer from the difficulties in rational handling due to the complicated procedures, and are thus not in favor of practical applications. It appears very important to explore some simple methods for $Li_4Ti_5O_{12}$ to work at high rates.

We assumed that defective mesoporous $Li_4Ti_5O_{12-y}$ could be an ideal electrode material at high rates, based on the following 3-fold considerations: (i) $Li_4Ti_5O_{12}$ has merits of cycling stability and safety; (ii) $Li_4Ti_5O_{12}$, when prepared in a defective structure, has abundant oxygen vacancies and Ti^{3+}-O-Ti^{4+} pairs, which can effectively enhance the electronic conductivity [12–15]; and (iii) $Li_4Ti_5O_{12}$, when prepared in a mesoporous structure, will have the shortened electron or lithium-ion transport pathways, which can decrease the polarization and further enhance the electrochemical performance at high rates [3,16]. Unfortunately, defective mesoporous $Li_4Ti_5O_{12-y}$ has not been reported till now, and thus it is not clear whether defective mesoporous $Li_4Ti_5O_{12-y}$ can work at high rates as promising as it does at low-rates.

In this work, we successfully prepared defective mesoporous $Li_4Ti_5O_{12-y}$ by initiating a facile solvothermal method with a subsequent N_2 treatment. Using this method, Ti^{3+} is first introduced into the mesoporous $Li_4Ti_5O_{12}$ to generate a defective structure with oxygen vacancies, which has led to an apparent increase in intrinsic electronic conductivity and furthermore an enhanced electrochemical performance. The resultant defective mesoporous $Li_4Ti_5O_{12-y}$ is found to work pretty well at a high rate of 20 C. The method reported here is novel, which does not need any aids from the

* Corresponding author. Tel.: +86 591 83702122; fax: +86 591 83702122.
E-mail address: guangshe@fjirsm.ac.cn (G. Li).

0378-7753/$ – see front matter © 2012 Elsevier B.V. All rights reserved.
doi:10.1016/j.jpowsour.2012.03.014

conductive layers or foreign dopants popularly used in previous literatures.

2. Experimental

Defective mesoporous $Li_4Ti_5O_{12-y}$ was prepared by developing a solvothermal method with a subsequent annealing in N_2. In a typical process, a suspension of 1.2 g glycine and 60 mL anhydrous ethanol was stirred for 1 h. A relatively stable suspension was then obtained by removing off the large glycine particles, and then 3 mL titanium *n*-butoxide ($Ti(OBu)_4$) and 0.296 g lithium hydroxide monohydrate ($LiOH{\cdot}H_2O$) were added slowly into the suspension, which was stirred for 3 h. The suspension was then transferred into a 100 mL autoclave and maintained at 200 °C for 20 h. The product was collected by filtration and washed with anhydrous ethanol for several times and dried at 80 °C. The sample was finally obtained by annealing the product in N_2 at 500 °C for 2 h, which gives the defective mesoporous sample: *LTO-N*. For comparison, a parallel sample preparation was done: stoichiometric mesoporous sample, *LTO-A* was synthesized under the similar conditions but treated in air.

Crystal structures of the samples were examined by X-ray diffraction (XRD) using a Rigaku MinFlex II benchtop X-ray diffiractometer with a copper target. The lattice parameters were calculated by a least-squares method. Morphology and crystalline structure of the samples were observed by field-emission scanning electron microscopy (FE-SEM, JEOL JSM-6700) and high-resolution transmission electron microscopy (HR-TEM, JEOL JEM-2010). Nitrogen adsorption–desorption isotherms were measured on Micromerities ASAP 2000 surface area and porosity analyzer. The pore size distribution and specific surface area of the sample were derived using the Barrett-Joyner-Halenda (BJH) model and the multipoint Braunauer-Emmett-Teller (BET) method, respectively. Electron paramagnetic resonance (EPR) spectra were recorded on a Bruker ELEXSYS E300 spectrometer at room temperature (X-band frequency, microwave power of 5.04 mW, and 9.86 GHz field modulation).

Total electrical conductivities of the samples were measured using alternating current impedance spectroscopy on an impedance analyzer (Agilent 4294A) in the frequency range of 40 Hz to 5 MHz at room temperature with an oscillation voltage of 0.5 V. The impedance data were analyzed by an equivalent circuit model using the Zsimpwin program. The electronic conductivities were determined using direct current measurement on a digital source meter (Keithley 2400). For all measurements, samples of given mounts were pressed uni-axially into pellets with a diameter of 7 mm and about 2 mm in thickness. Silver paste was painted onto both sides of pellets as electrodes. All pellets were tightly compressed at room temperature without sintering.

Electrochemical performance of the samples was characterized using CR2025 coin-type cells. The electrodes were fabricated by mixing the as-prepared $Li_4Ti_5O_{12-y}$ powders, acetylene black, and poly(vinylidene fluoride) at weight ratios of 70:15:15, respectively, using N-methyl pyrrolidone as a solvent. The slurry was then casted onto copper foil current collector and dried at 100 °C in vacuum. After the evaporation of the solvent, disks of 1.54 cm^2 were punched out of the foil. For comparison, the loadings of the samples on each disk were set at a similar level about 1.3 mg cm^{-2}. The cells were assembled in an Ar-filled glovebox by using lithium foil as the counter electrode and a polypropylene film as the separator. The electrolytes were 1 M $LiPF_6$ dissolved in ethyl carbonate (EC), diethyl carbonate (DEC) and dimethyl carbonate (DMC) in a volume ratio of 1:1:1. The cells were charged and discharged galvanostatically using a battery tester (Land Battery Test System) in a voltage range of 3.0-1.0 V (vs. Li^+/Li) at room temperature. Cyclic voltammetry were carried out on an electrochemical workstation (CHI660 C) between 3.0 V and 1.0 V at sweep rates varied from 0.6 to 1 mV s^{-1}.

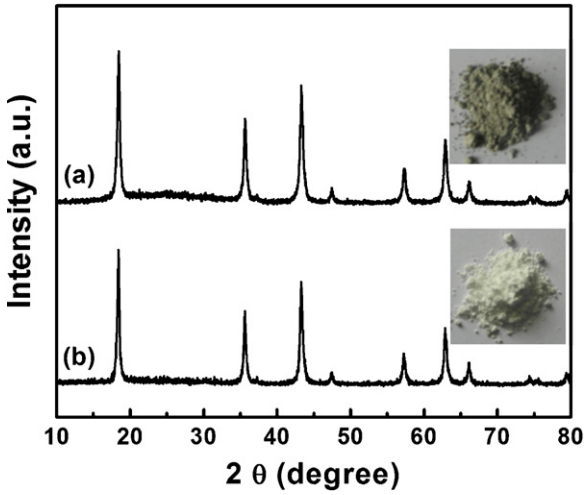

Fig. 1. XRD patterns of the samples: (a) LTO-N and (b) LTO-A. Insets show the corresponding sample colors.

To study the conductivity effect on cycle rates, 5 wt% carbon was mixed with the as-prepared LTO-N and LTO-A powders before electrode preparation, while other experimental conditions were maintained. The resultant samples of carbon mixed with LTO-N and LTO-A were named as LTO-N-C and LTO-A-C, respectively.

3. Results and discussion

Fig. 1 shows XRD patterns of the LTO-N and LTO-A samples. It is observed that all XRD peaks for the two samples are sharp, which indicates high crystallinity. Further, all these diffraction peaks are well indexed to a cubic spinel structure of $Li_4Ti_5O_{12}$ (space group: Fd3 m, JDPDS, No. 49-0207), while no other impurity phases are observed. Therefore, single-phase $Li_4Ti_5O_{12}$ with a high crystallinity is obtained for LTO-N and LTO-A. The chemical compositions for the samples were also analyzed by elemental analyzer. It is found that the residual carbon amount in LTO-N and LTO-A are as low as 0.76% and 0.66%, respectively. In spite of single phases and similar chemical compositions, the samples' colors are quite different: For LTO-N, the sample color is gray, which compared to the white color for LTO-A. It seems that Ti^{3+} and the relevant defects are present in LTO-N, as already indicated in a previous literature [15].

Morphologies and particle sizes for samples were examined by SEM and HRTEM. As indicated in Fig. 2a, sample LTO-N consists of submicron-size secondary quasi-spheres (100 - 500 nm) as accumulated by nanosized primary particles. These primary particles are further observed to have a dimension about 15-25 nm from the HRTEM images (Fig. 2b). The d-spacing for plane (111) is 0.48 nm, in good accordance with that previously reported for spinel $Li_4Ti_5O_{12}$ [17]. Further, as indicated by SEM and TEM images (Fig. 2c and 2d), LTO-A shows morphology and particle sizes quite similar to those of LTO-N. Namely, both samples were aggregates formed by nanosized primary particles with dimension of about 15-22 nm. The electron-diffraction patterns for LTO-N and LTO-A exhibit sharp spots (not shown). Therefore, both samples are demonstrated to have a high crystallinity.

Pore size distribution and BET surface area for samples LTO-N and LTO-A were investigated by N_2 adsorption/desorption analysis. From the pore size distribution curve in Fig. 3a, the average pore size for LTO-N is determined to be 3.6 nm, which is likely resulted from

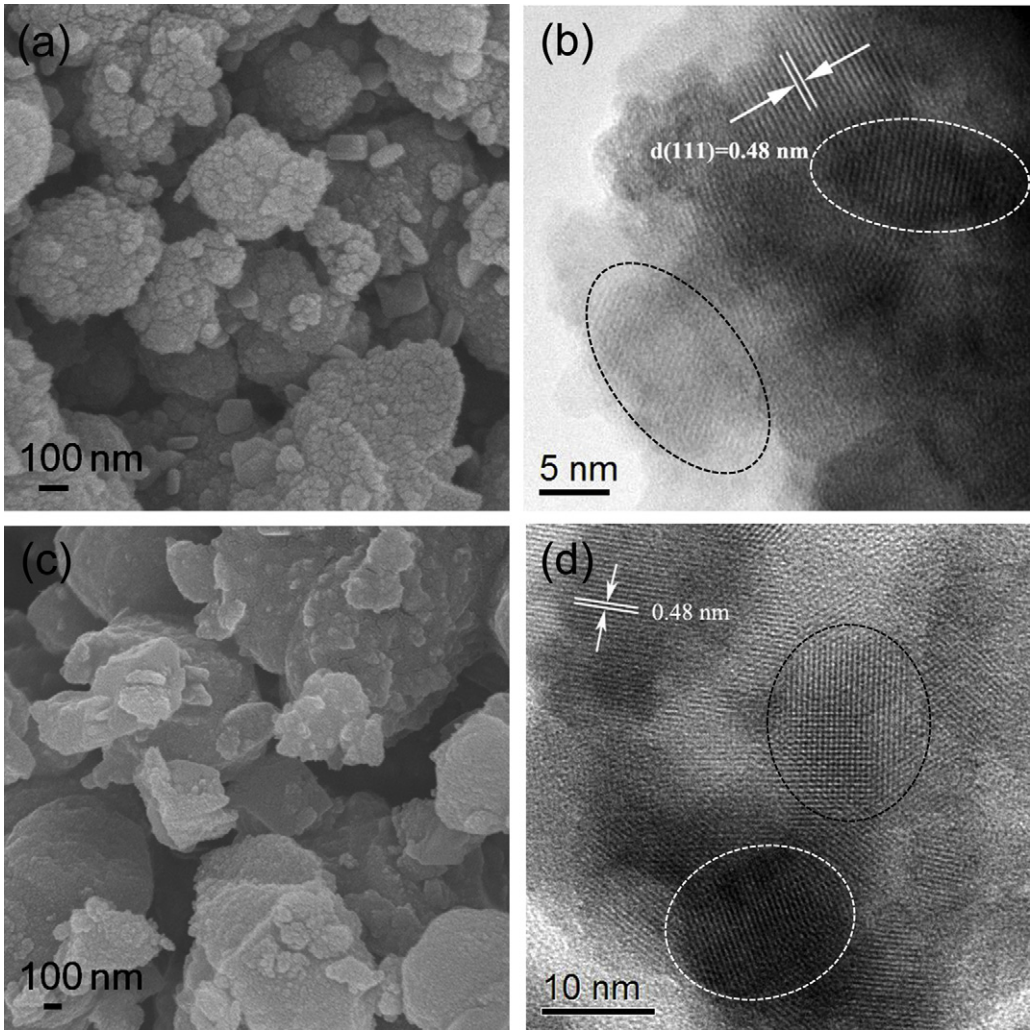

Fig. 2. (a) SEM and (b) HRTEM images for LTO-N; (c) SEM and (d) HRTEM images for LTO-A.

the accumulation of nanosized primary particles. Similar mesoporous feature is also observed for LTO-A. Surprisingly, the BET surface area of LTO-N is 30.1 $m^2 g^{-1}$, which is almost half of that for LTO-A (54.8 $m^2 g^{-1}$). According to popular thoughts, LTO-N may have worse electrochemical performance than LTO-A, since larger surface area can provide more efficient transport pathways to the interior voids with an increased electrode-electrolyte interfacial area critical for high-rate lithium ion batteries. Our electrochemical tests below will give a totally different result.

Defects of the samples were identified by EPR which is sensitive to the electrons and holes trapped at defect sites [18]. Fig. 4 shows

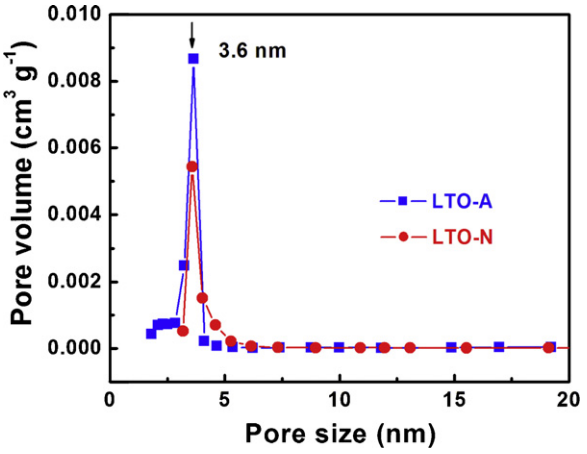

Fig. 3. Pore size distribution curves for LTO-N and LTO-A.

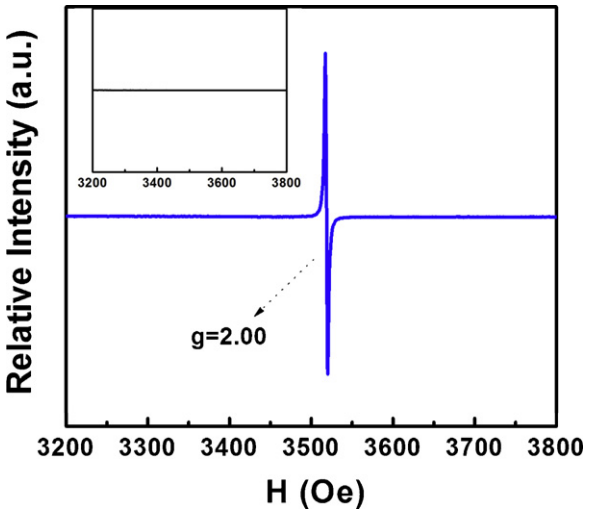

Fig. 4. EPR signals of LTO-N. Inset shows the EPR signals for LTO-A.

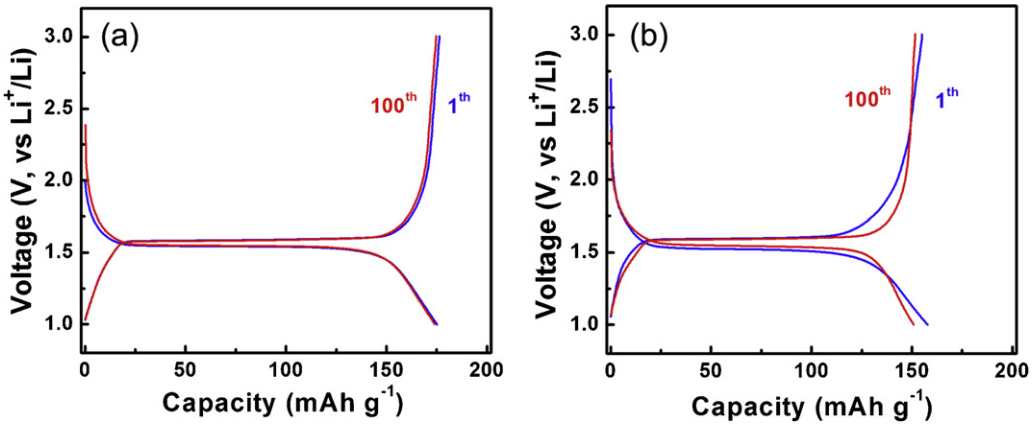

Fig. 5. Charge/discharge curves for (a) LTO-N and (b) LTO-A at a current density of 1 C.

the EPR spectrum for LTO-N. Only one intense signal is observed at about g = 2.00, which confirms the presence of oxygen vacancies and Ti^{3+} in LTO-N, as indicated in other Ti^{3+} containing systems [19]. Therefore, LTO-N is indicated to crystallize in a defective structure $Li_4Ti_5O_{12-y}$. Comparatively, LTO-A does not show any EPR signals for oxygen vacancies and Ti^{3+} (see inset of Fig. 4).

The presence of Ti^{3+} in LTO-N is also confirmed by lattice parameter comparison. For LTO-N, the lattice parameter is 0.83605 (±4) nm, which is slightly larger than that of 0.83595 (±3) nm for LTO-A. This can be understood, since Ti^{3+} has an ionic radium of 0.067 nm in 6-fold coordination, which is slightly larger than that of 0.0605 nm for Ti^{4+}. Then, Ti^{3+}-O-Ti^{4+} pairs are included in LTO-N, which may lead to an improved electronic conductivity as reported by others [12]. To confirm this, we compare the total electrical conductivities and electronic conductivities of both pellet samples LTO-N and LTO-A using alternating current impedance spectra and direct current method, respectively. The impedance data for both samples are semi-arcs through origin, which is associated with bulk conduction. The electrical conductivity thus obtained is 1.86×10^{-7} S cm^{-1} for LTO-N, which is closer to that of 1.48×10^{-7} S cm^{-1} for LTO-A. Comparatively, electronic conductivity for LTO-N is 1.47×10^{-8} S cm^{-1}, approximately five times higher than that of 2.78×10^{-9} S cm^{-1} for LTO-A. It is noted that, in the case of no carbon and/or foreign dopant involved, the intrinsic electronic conductivity as for pure $Li_4Ti_5O_{12}$ is usually extremely low, <10^{-13} S cm^{-1} as reported by Jansen and coworkers [6]. By subtracting the electronic conductivity from the total electrical conductivity, the ionic conductivity for LTO-N is estimated to be 1.71×10^{-7} S cm^{-1}, almost the same as that of 1.44×10^{-7} S cm^{-1} for LTO-A.

Fig. 5 shows the discharge/charge profiles of samples LTO-N and LTO-A at 1 C. Both samples show typical flat plateau around 1.55 V (vs. Li^+/Li), which corresponds to two-phase transition between $Li_4Ti_5O_{12}$ (spinel) and $Li_7Ti_5O_{12}$ (rock salt). However, LTO-N presents a more flat plateau profile and a larger plateau capacity than LTO-A. It should be noted that the potential difference between the charge and discharge plateau of LTO-N electrode is much smaller than that of the LTO-A electrode. It indicates that the LTO-N electrode has a lower polarization and better reaction kinetics. The discharge capacity for LTO-N is 175 mAh g^{-1} for the first cycle, and it still can remain 174 mAh g^{-1} over 100 cycles with capacity retention of 99%. The capacity for LTO-N over 100 cycles is very close to the theoretical capacity of $Li_4Ti_5O_{12}$ and superior to others reported for $Li_4Ti_5O_{12}$ in literature [20]. Comparatively, LTO-A delivers relatively lower capacity retention of 96.8% after 100 cycles with an initial discharge capacity of 158 mAh g^{-1}.

Defective mesoporous $Li_4Ti_5O_{12-y}$ is further investigated for possible high power applications by determining its rate capability under various current densities from 1 C to 50 C. As shown in Fig. 6, sample LTO-N delivers discharge capacities of 178, 172, 161, 146, 125, and 85 mAh g^{-1} at current densities of 1, 2, 5, 10, 20, and 50 C, respectively, while at the corresponding current densities, the capacities for LTO-A are poor, as represented by the values of 154, 141, 121, 96, 66, and 32 mAh g^{-1}. It is striking that at a high rate of 20 C, the defective mesoporous $Li_4Ti_5O_{12-y}$ still retained a high discharge capacity of 125 mAh g^{-1}, almost two times higher than the stoichiometric mesoporous counterpart. Such a high-rate performance is barely attained with or without any aids of conductive layers or doping foreign ions [16,21,22]. The capacity differences between LTO-N and LTO-A increased dramatically with increasing the discharge rate. For instance, the capacity of 125 mAh g^{-1} for LTO-N at high rate of 20 C was even higher than that of 121 mAh g^{-1} for LTO-A at a four times lower rate (5 C). To study the kinetics of lithium-ion diffusion, cyclic voltammetry was performed to measure lithium-ion diffusion coefficient of both samples. For the defective mesoporous $Li_4Ti_5O_{12-y}$, lithium-ion diffusion coefficient was estimated to be 1.26×10^{-10} cm^2 s^{-1}, which is much larger than that of 8.48×10^{-11} cm^2 s^{-1} for stoichiometric mesoporous counterpart. Since the particle sizes and morphologies of both samples are similar as indicated in Fig. 2, the lithium-diffusivity aided by intrinsic electronic conductivity might be attributed to the improved lithium- ion diffusion coefficient of defective mesoporous $Li_4Ti_5O_{12-y}$.

Fig. 7 shows the cycling performance of LTO-N and LTO-A at 20 C (before test at 20 C, the cell was first cycled at 1 C for 3 cycles). The

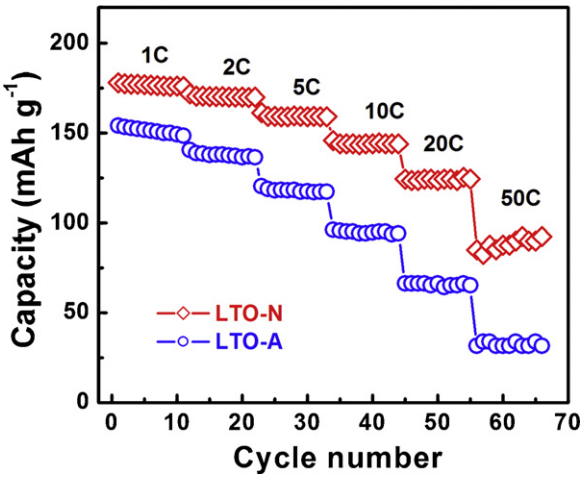

Fig. 6. Rate performance of LTO-N and LTO-A at various rates in a voltage window of 3.0-1.0 V (vs. Li^+/Li).

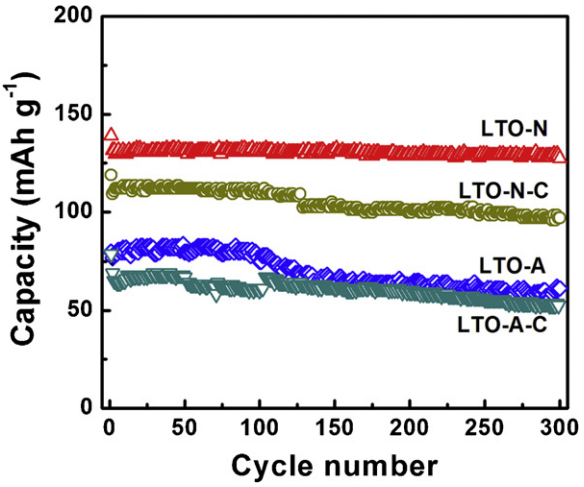

Fig. 7. Cycling performance of LTO-N and LTO-A at a high rate of 20 C in the potential range of 3.0–1.0 V. The relevant data for samples LTO-N-C and LTO-A-C were also given for comparison.

same current density was applied to the charge and discharge processes. It is clearly seen that LTO-N remains a high capacity with excellent capacity retention even at a high rate of 20 C. Namely, a discharge capacity of 139 mAh g^{-1} is obtained at the first cycle, while that after 300 cycles is still as high as 127 mAh g^{-1}, representing a capacity fading of 8.6%. The Coulombic efficiencies approached 100% even at the identical charge and discharge rates. It should be noted that such a long-term cycling performance at high rate of 20 C is barely achieved for $Li_4Ti_5O_{12}$ in literatures previously reported [16,23]. Instead, at the same rate of 20 C, LTO-A delivers a relatively lower discharge capacity of 80 mAh g^{-1} for the initial discharge capacity and worsened cycling stability of 23.8% capacity loss.

To further study the impacts of conductivity, LTO-N and LTO-A were mixed with more carbon, and the relevant cycling performance was measured. As indicated in Fig. 7, mixing more carbon decreased the discharge capacity and cycle stability of LTO-N and LTO-A. For example, in comparison with LTO-N, LTO-N-C delivered a lower initial discharge capacity of 118 mAh g^{-1} with an increase in capacity fading of 17.8% after 300 cycles. LTO-A-C delivered a lowest initial discharge capacity of 79 mAh g^{-1} with a largest capacity fading of 34.2%. This observation is out of expectation, since mixing more carbon may promote the electronic conduction across interfaces of LTO-N or LTO-A, which seems helpful to improve the electrochemical performance. In fact, the presence of excess surface carbon layers would retard lithium-diffusivity, and especially at high rate of 20 C, surface carbon layers might be peeled off from the surfaces of LTO-N or LTO-A, all of which are unfavorable for increasing the cycle rates. It deserves further systematic investigation in the future to get insight into the electrochemical behaviors of carbon species coated on the defective $Li_4Ti_5O_{12-y}$.

Having these experimental results in mind, one question appeared: What is the primary reason for superior electrochemical performance of LTO-N to that of LTO-A. To answer this question, one has to take into account several factors that may contribute to the electrochemical performance. For instance, particle size effect is popularly considered to be crucial for the electrochemical performance. For the present work, particle size effect can be first dismissed, since LTO-N and LTO-A show similar particles sizes and morphologies. The effect of surface areas can also be dismissed because it cannot rationalize why LTO-N with a smaller surface area of 30.1 $m^2 g^{-1}$ offers a higher performance than LTO-A with a larger surface area of 54.8 $m^2 g^{-1}$. Alternatively, intrinsic electronic conductivity should be highly concerned. As stated above, either total electrical conductivities or ionic conductivities for both samples are quite similar, while the electronic conductivity for LTO-N is approximately five times higher than that of LTO-A. It is most likely that the superior electrochemical performance of defective mesoporous $Li_4Ti_5O_{12-y}$ at high rates can be the consequence of enhanced electronic conductivity from the defective structures with oxygen vacancies and Ti^{3+}–O–Ti^{4+} pairs, which may aid the lithium-diffusivity for electrochemical performance.

We are aware that such an outstanding long-term electrochemical performance is barely reported at high rate of 20 C for $Li_4Ti_5O_{12}$, except for nanosized $Li_4Ti_5O_{12}$ with additional aids from hybridization with graphene[23]. Here we would like to briefly summarize the superior electrochemical performance for our defective mesoporous $Li_4Ti_5O_{12-y}$ at a high rate of 20 C: a discharge capacity of 139 mAh g^{-1} at the first cycle and 127 mAh g^{-1} after 300 cycles, capacity retention >91%, which are all comparable with those for nanosized $Li_4Ti_5O_{12}$/graphene hybrid materials recently reported [23], but much better than those for Zr^{2+} doped $Li_4Ti_5O_{12}$ [24], carbon coated $Li_4Ti_5O_{12}$ [25], porous $Li_4Ti_5O_{12}$ [22], nanosized or microsphere $Li_4Ti_5O_{12}$ [26–28]. Among the latter cases, nanosized $Li_4Ti_5O_{12}$ prepared by supercritical hydrothermal synthesis shows a capacity fading of about 16% with capacity of 116 mAh g^{-1} after 20 cycles at 20 C; Zr-doped $Li_4Ti_5O_{12}$ prepared by solid-state reaction shows a discharge capacity of 118 mAh g^{-1} at 20 C, and carbon coated $Li_4Ti_5O_{12}$ delivers a lower capacity of 110 mAh g^{-1} at the same rate.

4. Conclusions

Defective mesoporous $Li_4Ti_5O_{12-y}$ was synthesized via a solvothermal method with a subsequent annealing treatment in N_2. The resultant $Li_4Ti_5O_{12-y}$ showed an excellent rate performance and cycleability as represented by a capacity of 139 mAh g^{-1} at a high rate of 20 C and capacity retention of 91.4% over 300 cycles. The outstanding electrochemical performance can be ascribed to the enhanced intrinsic electronic conductivity from the defective structures with oxygen vacancies and Ti^{3+}–O–Ti^{4+} pairs. The findings reported in this work may help to find facile approaches to greatly improve the electrochemical performance of $Li_4Ti_5O_{12}$ for uses in high-rate lithium-ion batteries.

Acknowledgements

This work was financially supported by NSFC under the contract (Nos. 21025104, 91022018, and 20831004), 973 project (No. 2011CB935904), and FJIRSM fund (No. 2010KL002).

References

[1] V. Etacheri, R. Marom, R. Elazari, G. Salitra, D. Aurbach, Energy and Environmental Science 4 (2011) 3243–3262.
[2] H.S. Fang, Z.Y. Pan, L.P. Li, Y. Yang, G.F. Yan, G.S. Li, S.Q. Wei, Electrochemistry Communications 10 (2008) 1071–1073.
[3] G.N. Zhu, H.J. Liu, J.H. Zhuang, C.X. Wang, Y.G. Wang, Y.Y. Xia, Energy and Environmental Science 4 (2011) 4016–4022.
[4] G.F. Yan, H.S. Fang, H.J. Zhao, G.S. Li, Y. Yang, L.P. Li, Journal of Alloys and Compounds 470 (2009) 544–547.
[5] L.F. Shen, C.Z. Yuan, H.J. Luo, X.G. Zhang, S.D. Yang, X.J. Lu, Nanoscale 3 (2011) 572–574.
[6] C.H. Chen, J.T. Vaughey, A.N. Jansen, D.W. Dees, A.J. Kahaian, T. Goacher, M.M. Thackeray, Journal of the Electrochemical Society 148 (2001) A102–A104.
[7] Y.G. Wang, H.Q. Li, P. He, E. Hosono, H.S. Zhou, Nanoscale 2 (2010) 1294–1305.
[8] E.M. Sorensen, S.J. Barry, H.K. Jung, J.R. Rondinelli, J.T. Vaughey, K.R. Poeppelmeier, Chemistry of Materials 18 (2006) 482–489.
[9] T.F. Yi, J. Shu, Y.R. Zhu, X.D. Zhu, R.S. Zhu, A.N. Zhou, Journal of Power Sources 195 (2010) 285–288.
[10] D. Dambournet, I. Belharouak, J.W. Ma, K. Amine, Journal of Power Sources 196 (2011) 2871–2874.
[11] H.L. Zhao, Y. Li, Z.M. Zhu, J. Lin, Z.H. Tian, R.L. Wang, Electrochimica Acta 53 (2008) 7079–7083.
[12] J. Wolfenstine, U. Lee, J.L. Allen, Journal of Power Sources 154 (2006) 287–289.

[13] H.G. Jung, S.T. Myung, C.S. Yoon, S.B. Son, K.H. Oh, K. Amine, B. Scrosati, Y.K. Sun, Energy and Environmental Science 4 (2011) 1345–1351.
[14] K.S. Park, A. Benayad, D.J. Kang, S.G. Doo, Journal of the American Chemical Society 130 (2008) 14930–14931.
[15] Y.G. Wang, H.M. Liu, K.X. Wang, H. Eiji, Y.R. Wang, H.S. Zhou, Journal of Materials Chemistry 19 (2009) 6789–6795.
[16] Y.F. Tang, L. Yang, Z. Qiu, J.S. Huang, Journal of Materials Chemistry 19 (2009) 5980–5984.
[17] L.F. Shen, C.Z. Yuan, H.G. Luo, X.G. Zhang, K. Xu, Y.Y. Xia, Journal of Materials Chemistry 20 (2010) 6998–7004.
[18] L.P. Li, G.S. Li, J.X. Xu, J. Zheng, W.M. Tong, W.B. Hu, Physical Chemistry Chemical Physics 12 (2010) 10857–10864.
[19] S.Q. Zhou, E. Čižmár, K. Potzger, M. Krause, G. Talut, M. Helm, J. Fassbender, S. Zvyagin, J. Wosnitza, H. Schmidt, Physical Review B 79 (2009) 113201.
[20] L. Cheng, J. Yan, G.N. Zhu, J.Y. Luo, C.X. Wang, Y.Y. Xia, J. Mater. Chem. 20 (2010) 595–602.
[21] J.J. Huang, Z.Y. Jiang, Electrochem. Solid State Lett. 11 (2008) A16–A18.
[22] K.C. Hsiao, S.C. Liao, J.M. Chen, Electrochimica Acta 53 (2008) 7242–7247.
[23] Y. Shi, L. Wen, F. Li, H.M. Cheng, Journal of Power Sources 196 (2011) 8610–8617.
[24] X. Li, M. Qu, Z. Yu, Journal of Alloys and Compounds 487 (2009) L12–L17.
[25] T. Yuan, R. Cai, Z.P. Shao, Journal of Physical Chemistry C 115 (2011) 4943–4952.
[26] A. Nugroho, S.J. Kim, K.Y. Chung, B.W. Cho, Y.W. Lee, J. Kim, Electrochemistry Communications 13 (2011) 650–653.
[27] S.L. Chou, J.Z. Wang, H.K. Liu, S.X. Dou, Journal of Physical Chemistry C 115 (2011) 16220–16227.
[28] T. Yuan, R. Cai, P. Gu, Z.P. Shao, Journal of Power Sources 195 (2010) 2883–2887.